

Intrinsic anomalous Hall effect arising from antiferromagnetic structure revealed by high-quality NbMnP

Yuki Arai^{1*}, Junichi Hayashi², Keiki Takeda², Hideki Tou¹, Hitoshi Sugawara¹, and Hisashi Kotegawa¹

¹Department of Physics, Kobe University, Kobe, Hyogo 657-8501, Japan

²Muroran Institute of Technology, Muroran, Hokkaido 050-8585, Japan

The large anomalous Hall effect (AHE) in antiferromagnetic (AF) materials arises from symmetry breaking equivalent to a ferromagnetic (FM) state. Consequently, this suggests that the observed AHE is induced by the intrinsic mechanism of the band structure effect, which in turn induces dissipationless transverse conductivity. Confirmation of impurity-insensitive anomalous Hall conductivity (AHC) is crucial to conclude this interpretation; however, experimental investigations in AF materials are limited by the lack of high quality systems. In this study, we show that the AF material NbMnP, which exhibits a large AHE, offers a high quality single crystal. Our findings clearly revealed that the large AHC and the tiny net magnetization of $\sim 10^{-3}\mu_B/\text{Mn}$ are inherent in this material, irrespective of disorder. NbMnP is a novel AF material that generates FM responses in the regime where there is less impurity scattering.

arXiv:2403.05058v1 [cond-mat.mes-hall] 8 Mar 2024

Interpretation of the anomalous Hall effect (AHE) has been a long term controversial issue in condensed matter physics.¹⁾ Earlier, Karplus and Luttinger proposed that an external electric field induces anomalous transverse velocity through spin-orbit interactions.²⁾ Consequently, since this is a band-structure effect, anomalous Hall conductivity (AHC) is expected to be independent of any impurity scattering, and this mechanism is called an intrinsic AHE. However, impurity scattering, which has been recognized as skew scattering or side-jump scattering, has also been shown to trigger AHE, i.e., extrinsic AHE.^{3,4)} The absence of an intuitive explanation for the dissipationless intrinsic AHE has prevented it from becoming mainstream for the interpretation of AHE; however, in the 2000s, the intrinsic AHE was reconstructed using a Berry phase concept, and the first-principle calculation enabled researchers to obtain the theoretical value of AHC.^{1,5-7)} Currently, there are two widely recognized methods to assess the origin of AHE. The first involves a comparison between the experimental and calculated AHCs.^{6,7)} However, accurate calculations under the magnetically-ordered state are required. The second is to investigate the impurity-scattering dependence of the AHC. Although this is not related to the validity of the above theoretical calculation, relatively clean samples are needed because the expected tendency for the intrinsic mechanism appears only in the moderate conductivity regime.⁸⁾

A success introduced by the Berry phase concept was the discovery of a large AHE arising from an antiferromagnetic (AF) structure,^{9,10)} which can occur when the magnetic point group of the AF state allows ferromagnetic (FM) states. After the discovery of a large AHE in Mn_3Sn ,¹⁰⁾ several AF materials exhibited AHE at zero fields accompanied by tiny net magnetization.¹¹⁻¹⁴⁾ The consistency between experimental and theoretical values of AHC presented by previous studies through band-structure calculations in some materials confirmed that AF structures induce the intrinsic AHE.^{10-12,15,16)} However, another important experimental confirmation regarding impurity-scattering dependence has not yet been sufficiently investigated for AF materials, because it has been

difficult to control impurity scattering owing to the lack of high-quality crystals. In fact, their residual resistivity ratios (RRRs) have been attained only for ~ 2 -3 for Mn_3Sn , Mn_3Ge , NbCo_3S_6 , and TaCo_3S_6 . For α -Mn, a crystal with $\text{RRR} = 17$ can be obtained, and confirmation of the impurity-scattering dependence of the AHE has been performed;¹⁷⁾ however, the magnetic structure under pressure, which yields AHE, remains unclear.

Recently, we identified a large AHE in the noncollinear AF material NbMnP.¹⁸⁾ The AF structure of NbMnP, which is illustrated using VESTA,¹⁹⁾ is represented by a combination of the magnetic point group $mm'm$ (irreducible representation B_{2u}) and $mm'm'$ (B_{3g}), as shown in Fig. 1.²⁰⁾ $mm'm$ (B_{2u}) does not possess space-inversion symmetry (\mathcal{P}) and time reversal

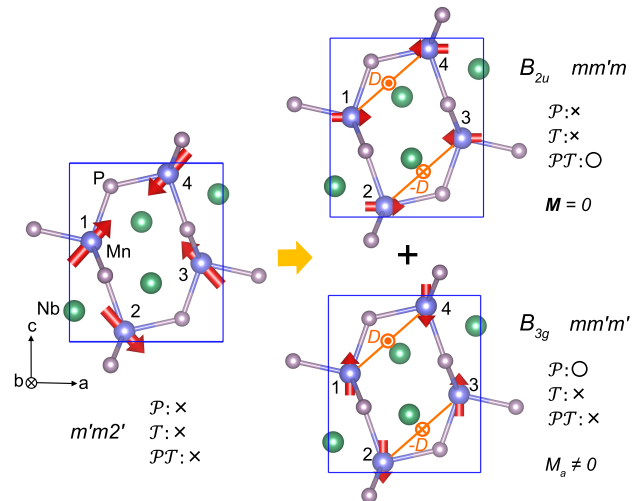


Fig. 1. The $Q = 0$ AF structure of NbMnP, which is represented by a linear combination of two irreducible representation.²⁰⁾ The unit cell includes four Mn atoms labeled Mn1-Mn4, which are equivalent in the paramagnetic state. This combination lowers the symmetry from $Pnma$ to $Pmn2_1$. The actual magnetic point group is $m'm2'$. In the B_{2u} component, \mathcal{PT} symmetry protects the compensated AF structure, even though the Dzyaloshinskii-Moriya (DM) interaction works. In the \mathcal{PT} -symmetry broken B_{3g} component, the DM interaction induces magnetization along the a axis.

*222s102s@stu.kobe-u.ac.jp

symmetry (\mathcal{T}), but instead maintains the \mathcal{PT} symmetry. In $mm'm'$ (B_{3g}), which is represented by a magnetic toroidal quadrupole,²¹⁾ \mathcal{PT} -symmetry is broken, and it can thus induce AHE even from the AF structure, because it symmetrically allows FM components along the a -axis. The observed AHC of $\sigma_H = 230 \Omega^{-1}\text{cm}^{-1}$ was almost consistent with the theoretical AHC of $\sigma_H = 273 \Omega^{-1}\text{cm}^{-1}$.¹⁸⁾ This consistency supports the intrinsic nature of AHE. In contrast, the impurity-scattering dependence of σ_H has not been verified even in NbMnP because its RRR value was 2, as well as in other AF materials showing the AHE.¹⁰⁻¹⁴⁾ High-quality single crystals of NbMnP need to be used to confirm the origin of the AHE.

In this Letter, we report the single-crystal growth of NbMnP using a Ga-flux method, which is different from the previous self-flux method.¹⁸⁾ The RRR of the new crystals exceeded 40, which was much higher than the value of 2 obtained in our previous study, indicating a drastic improvement in sample quality. The high-quality NbMnP also showed a large AHE, whose AHC was almost comparable to that of the previously used crystal with low RRR. These results suggest that the AHE in NbMnP arises intrinsically from the band structure under the AF spin configuration.

For the Ga flux method, a mixture of Nb, Mn, P, and Ga in a molar ratio of 1 : 1 : 1 : 30, respectively, was placed in an Al_2O_3 crucible and sealed in an evacuated quartz ampoule. We gradually heated the ampoule to 1050 °C and held it at this temperature for 72 hours, followed by slow cooling to 650 °C at -5 °C/h. After centrifugation, we obtained needle-like single crystals. Crystal symmetry and lattice parameters were determined by single-crystal X-ray diffraction measurements using a Rigaku Saturn724 Diffractometer with a multilayer mirror monochromated Mo- K_α radiation at room temperature. We measured both electrical and Hall resistivity using a standard four-probe method, and we antisymmetrized the Hall resistivity against magnetic fields to remove the longitudinal component induced by contact misalignment. Furthermore, we measured the magnetic properties using a commercial SQUID magnetometer and fixed several pieces of the crystals.

Figure 2(a) and (b) show a comparison of the electrical resistivity (ρ_{yy}) for different crystals. Here, x , y , and z correspond to a , b , and c -axes, respectively. The ρ_{yy} demonstrates kinks at $T_N = 233$ K for the self-flux crystals and at 244 K for the Ga-flux crystal. A drastic change appears in the residual resistivity: RRR = 2 for the self-flux crystal (Sample 1: S_1) and RRR = 42 for the Ga-flux crystal (Sample 3: S_3), clearly showing that the Ga-flux method is highly effective for obtaining high quality single crystals of NbMnP. T_N increased by ~ 10 K, accompanied by an improvement in sample quality. Figures 2(c) and 2(d) show a comparison of the magnetization curves at 2 K. In the self-flux NbMnP with lower RRR, a weak FM component of approximately $10^{-3}\mu_B/\text{Mn}$ appeared,¹⁸⁾ which was perpendicular to the b -axis.²²⁾ The high-quality NbMnP also shows an FM component of the same order of $10^{-3}\mu_B/\text{Mn}$, indicating that the net magnetization does not originate from poor sample quality but intrinsically. This also supports the interpretation that weak net magnetization originates from spin canting through the DM interaction.¹⁸⁾ As shown in Fig. 1, the DM interaction works between the two Mn atoms via AF coupling. The DM vectors for these couplings are directed along the b -axis, inducing spin

Table I. Structural parameters of NbMnP for two crystals obtained by the self-flux²⁰⁾ and the Ga flux methods, respectively, determined by single-crystal X-ray diffraction measurements at $T = 293$ K. The Wyckoff positions of all atoms were 4c, and all clear differences are underlined. The occupancy (Occ.) of the Nb site was improved by using the Ga-flux method.

NbMnP	self-flux	293 K	
Nb	Mn	P	
x	0.03102(5)	0.14147(9)	0.26798(15)
y	0.25000	0.25000	0.25000
z	0.67215(5)	0.05925(8)	0.36994(13)
Occ.	<u>0.968</u>	1	1
$U(\text{\AA}^2)$	0.00582(15)	0.0063(2)	0.0061(2)

Orthorhombic ($Pnma$)

$$a=6.1823(2) \text{\AA}, b=3.5573(2) \text{\AA}, c=7.2187(3) \text{\AA}, R=1.90\%$$

NbMnP	Ga flux	293 K	
Nb	Mn	P	
x	0.03122(7)	0.14162(12)	0.2682(2)
y	0.25000	0.25000	0.25000
z	0.67214(6)	0.05941(10)	0.37019(19)
Occ.	<u>0.995</u>	1	1
$U(\text{\AA}^2)$	0.0052(3)	0.0059(4)	0.0059(4)

Orthorhombic ($Pnma$)

$$a=6.1899(2) \text{\AA}, b=3.5478(1) \text{\AA}, c=7.2380(2) \text{\AA}, R=3.18\%$$

canting in the ac plane, because these bonds lie in the mirror plane. Note that there is no DM interaction between Mn1 and Mn3 (or Mn2 and Mn4) because of the inversion symmetry of the crystal. Spin canting through the DM interactions does not yield net magnetization in the B_{2u} representation with \mathcal{PT}

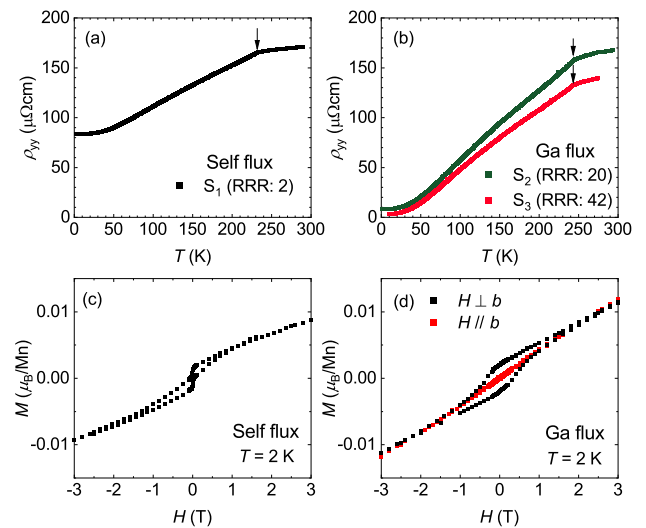


Fig. 2. Temperature dependence of electrical resistivity (ρ_{yy}) for (a) a self-flux crystal and (b) a Ga-flux crystal. The drastic enhancement of RRR ensures that the Ga-flux method is effective in obtaining high quality crystals. Magnetization curves at 2 K for (c) many pieces of unoriented self-flux crystals¹⁸⁾ and (d) aligned Ga-flux crystals. The similar spontaneous magnetization irrespective of the sample quality suggests that they are both inherent in NbMnP.

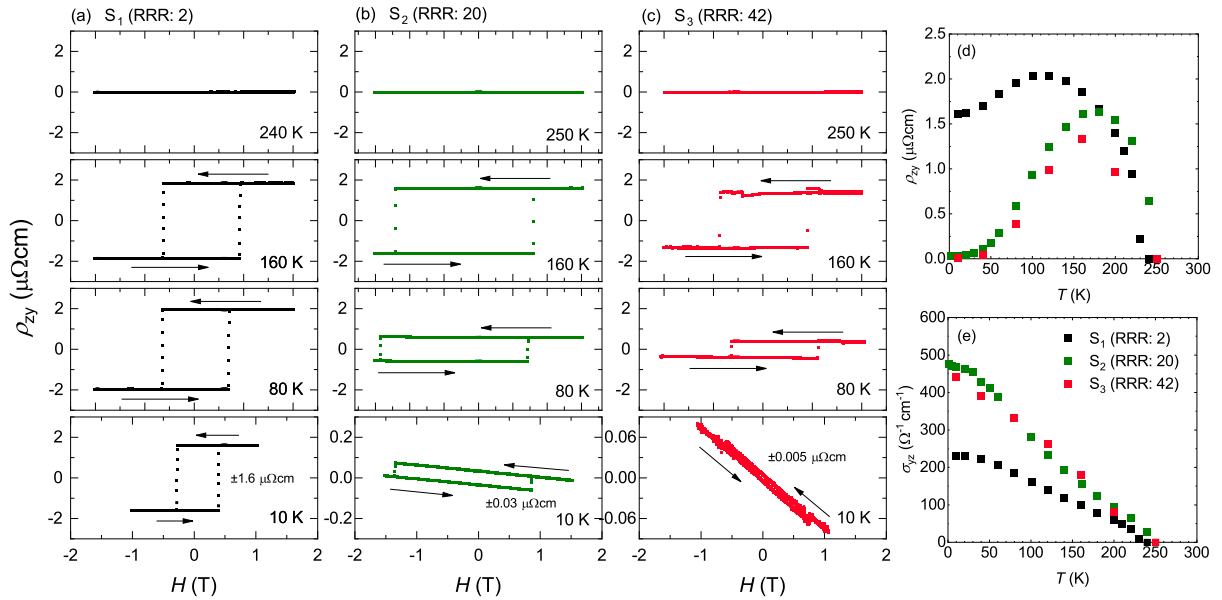


Fig. 3. (a-c) Field dependence of Hall resistivity ρ_{zy} for crystals with different RRRs. AHE shows hysteresis against the positive and negative magnetic fields and appears below T_N for all crystals. For RRR = 2, the large AHE remains at low temperatures, while it is suppressed, and the ordinary Hall effect becomes remarkable as RRR increases. For all crystals, measurements were performed after zero-field cooling to suppress the exchanged-bias effect of the material.¹⁸⁾ (d) Temperature dependence of ρ_{zy} at zero fields, i.e., the AHE component. (e) Temperature dependence of the AHC σ_{yz} , which was converted through $\sigma_{yz} \approx \rho_{zy}/\rho_{yy}^2$. A two times larger σ_{yz} was obtained for the Ga flux (S_2 and S_3) crystals compared with the self-flux crystal (S_1), while these values were similar between RRR = 20 and 42.

symmetry, because the AF couplings between Mn1 and Mn3 (or Mn2 and Mn4) are protected. For the \mathcal{PT} -symmetry broken B_{3g} representation, the DM interaction induces nonzero net magnetization along the a -axis.

We then evaluated the crystallographic differences between the two types of crystals using single-crystal X-ray diffraction measurements. The results are shown in Table I. It is shown that although the space group remains the same, the b -axis length slightly shrinks and the c -axis length becomes enlarged for the Ga-flux crystal. A significant difference appears in the occupancy at the Nb site, which showed nonnegligible deficiency in the self-flux crystal. The deficiency at the Nb site almost disappears for the Ga-flux crystal, suggesting that the improvement of the stoichiometry was achieved by using the Ga-flux method.

Figures 3(a-c) show the Hall resistivity ρ_{zy} for three crystals with RRR = 2, 20, and 42. Here, magnetic fields were applied along the a -axis to align the AF domains. The emergence of hysteresis below T_N indicates that all crystals exhibited zero-field AHE in the magnetically ordered state. The positive (negative) magnetic field selects the AF domain, generating the positive (negative) ρ_{zy} , respectively, and generating hysteresis. At 160 K, the magnitudes of ρ_{zy} 's were similar among the three crystals, while they were strongly suppressed toward low temperatures in the high quality crystal, where the field-dependent ordinary Hall effect is remarkable compared with the AHE. Despite the fact that both the width of the hysteresis and the exchange-bias effect¹⁸⁾ depend on the crystals, the tendency remains unclear at present. The suppression of ρ_{zy} is clearly observed in the temperature dependence of ρ_{zy} , as shown in Fig. 3(d). This behavior is simply explained by a difference in sample quality, i.e., a difference in electrical resistivity. In general, ρ_{zy} is connected to Hall conductivity through $\sigma_{yz} \approx \rho_{zy}/\rho_{yy}\rho_{zz}$. When the band struc-

ture determines the dissipationless Hall conductivity σ_{yz} of the sample quality, ρ_{zy} highly depends on the electrical resistivity, thereby reflecting the sample quality. We obtained σ_{yz} through $\sigma_{yz} \approx \rho_{zy}/\rho_{yy}^2$, and plotted them in Fig. 3(e). The σ_{yz} was found to continuously increase toward low temperatures for all crystals. The values at the lowest temperature were $230 \Omega^{-1}\text{cm}^{-1}$ for RRR = 2 and $\sim 450 \Omega^{-1}\text{cm}^{-1}$ for RRR = 20 and 42, thereby demonstrating an approximately twofold difference among the crystals; however, this difference is still small compared with the difference of 20 times in RRR.

To assess the impurity-scattering dependence of the AHC, Fig. 4(b) presents the plots of ρ_H ($= \rho_{zy}$) vs. ρ ($= \rho_{yy}$) in Fig. 4(a) and σ_H ($= \sigma_{yz}$) vs. σ ($= \sigma_{yy}$) for each NbMnP crystal. Below approximately 50 K, ρ_{zy} follows ρ^2 ; therefore, σ_{yz} is close to becoming constant against σ . These relationships experimentally demonstrate that the observed AHE arises through an intrinsic mechanism.¹⁾ This could not be confirmed using the previous low-quality crystal S_1 because of the weak temperature dependence of ρ and σ . In Fig. 4(c), we present $|\sigma_H|$ vs. σ for many ferromagnets,^{8, 23-28)} Mn_3X ($X = \text{Sn}$ and Ge),²⁹⁾ and NbMnP. Rich experimental data for ferromagnets demonstrate that σ_H is independent of σ in the intermediate conductivity region of $10^4 < \sigma < 10^6 \Omega^{-1}\text{cm}^{-1}$. In the dirty region of $\sigma < 10^3$ - $10^4 \Omega^{-1}\text{cm}^{-1}$, $\sigma_H \sim \sigma^{1.6}$ has been established,⁸⁾ while $\sigma_H \sim \sigma$ due to the skew scattering is expected to be dominant in the high conductivity region due to skew scattering. For AF materials, Mn_3X remains at around $10^4 \Omega^{-1}\text{cm}^{-1}$ in the intermediate region,²⁹⁾ while NbMnP covers a wide σ range of more than one order. The weak σ dependence of σ_H observed in the logarithmic scale resembles the behavior of ferromagnets, ensuring that the AHE under the AF structure is dominated by the intrinsic mechanism in the same framework as that of ferromagnets.

As future prospects, the benefit of obtaining high qual-

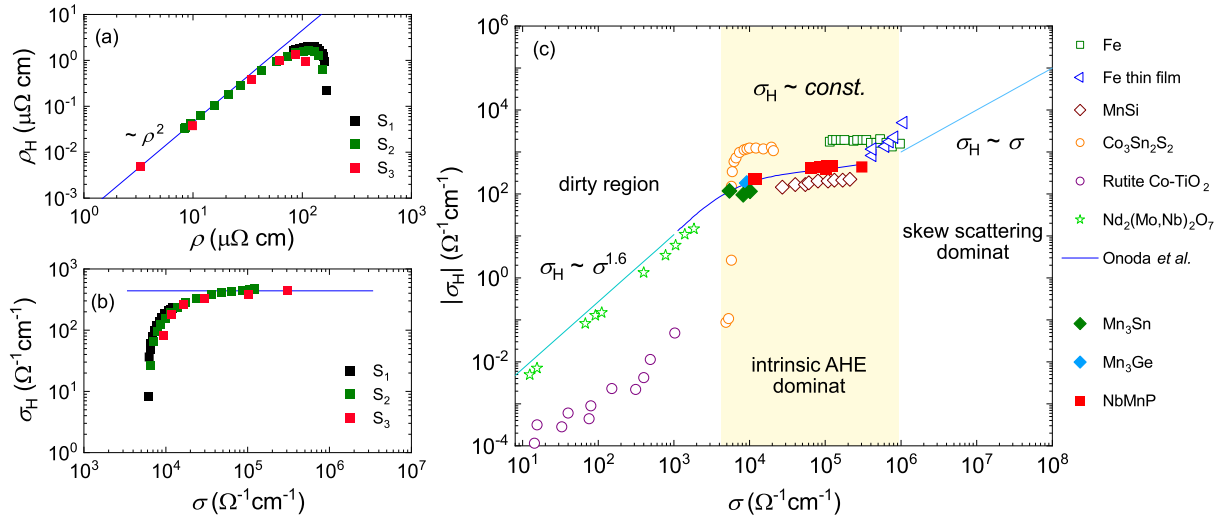


Fig. 4. Scaling relations in NbMnP between (a) anomalous Hall resistivity, $\rho_H (= \rho_{zy})$ and longitudinal electrical resistivity, $\rho (= \rho_{yy})$, and (b) AHC, $\sigma_H (= \sigma_{yz})$ and longitudinal conductivity, $\sigma (= \sigma_{yy})$. At temperatures below ~ 50 K, ρ_H obeys $\sim \rho^2$, and σ_H approaches constant values against σ . These behaviors suggest that the observed AHE mainly arises from the band structure effect without dissipation. (c) Scaling relation for many ferromagnets,^{8,23–28} Mn_3X ($X = Sn$ and Ge),²⁹ and NbMnP. The ferromagnets are displayed by open symbols, whereas the AF materials are represented by closed symbols. The data below ~ 50 K are plotted for NbMnP, showing a weak σ dependence in the wide conductivity region. The blue curve indicates the theoretical expectation with an appropriate amount of impurity.⁸

ity NbMnP is not intended for understanding AHE. The AF structure in the FM point group also generates FM responses such as an anomalous Nernst effect (ANE).^{30,31} The influence of disorder on ANE has not been well investigated even for ferromagnets, and thus impurity dependence is important for its understanding.³² Our preliminary experiment confirmed the emergence of ANE in NbMnP, which is a suitable material for assessing how impurities affect the ANE under the AF spin configuration. Another pathway is the elucidation of the asymmetric hysteresis, which appeared after field cooling in NbMnP.¹⁸ This exchange-bias effect is usually observed in artificial bilayers of FM and AF materials,^{33,34} and similar behavior has been observed in $Co_3Sn_2S_2$ ³⁵ and sample-size dependent.³⁶ In NbMnP, we speculated that the Nb deficiency affects its asymmetry through the pinning of the magnetic moments near the deficiency.¹⁸ This study showed that asymmetry still appeared, especially for the crystal with RRR = 20. Further investigations are needed, but careful disorder dependence is crucial.

In summary, we report that high quality NbMnP crystals with RRR > 40 were effectively obtained using the Ga-flux method. These crystals showed small net magnetization and large AHC, which were comparable to those found in the previous low quality crystal, revealing that both effects arise from intrinsic mechanisms. NbMnP single crystals, which cover a wide range of electrical conductivities, offer opportunities to systematically investigate the influence of disorder on FM responses arising from the AF spin configuration.

Acknowledgements

This work was supported by JSPS KAKENHI Grant Nos. 21K03446, 23H04871, and Murata Science Foundation.

- 2) R. Karplus and J. M. Luttinger, Phys. Rev. **95**, 1154 (1954).
- 3) J. Smit, Physica **24**, 39 (1958).
- 4) L. Berger, Phys. Rev. B **2**, 4559 (1970).
- 5) F. D. M. Haldane, Phys. Rev. Lett. **93**, 206602 (2004).
- 6) Z. Fang, N. Nagaosa, K. S. Tahakashi, A. Asamitsu, R. Mathieu, T. Ogasawara, H. Yamada, M. Kawasaki, Y. Tokura, and K. Terakura, Science **302**, 92 (2003).
- 7) Y. Yao, L. Kleinman, A. H. MacDonald, J. Sinova, T. Jungwirth, D. Wang, E. Wang, and Q. Niu, Phys. Rev. Lett. **92**, 037204 (2004).
- 8) S. Onoda, N. Sugimoto, and N. Nagaosa, Phys. Rev. B **77**, 165103 (2008).
- 9) H. Chen, Q. Niu, and A. H. MacDonald, Phys. Rev. Lett. **112**, 017205 (2014).
- 10) S. Nakatsuji, N. Kiyohara, and T. Higo, Nature **527**, 212 (2015).
- 11) N. Kiyohara, T. Tomita, and S. Nakatsuji, Phys. Rev. Appli. **5**, 064009 (2016).
- 12) A. K. Nayak, J. E. Fischer, Y. Sun, B. Yan, J. Karel, A. C. Komarek, and C. Shekhar, N. Kumar, W. Schnelle, J. Kubler, C. Felser, and S. S. Parkin, Sci. Adv. **2**, e1501870 (2016).
- 13) N. J. Ghimire, A. S. Botana, J. S. Jiang, J. Zhang, Y.-S. Chen, and J. F. Mitchell, Nat. Commun. **9**, 3280 (2018).
- 14) P. Park, Y.-G. Kang, J. Kim, K. H. Lee, H.-J. Noh, M. J. Han, and J.-G. Park, npj Quantum Materials **7**, 42 (2022). 4.2
- 15) J. Küber and C. Felser, EPL **108**, 67001 (2014).
- 16) M.-T. Suzuki, T. Koretsune, M. Ochi, and R. Arita, Phys. Rev. B **95**, 094406 (2017).
- 17) K. Akiba, K. Iwamoto, T. Sato, S. Araki, and T. C. Kobayashi, Phys. Rev. Reser. **2**, 043090 (2020).
- 18) H. Kotegawa, Y. Kuwata, V. T. N. Huyen, Y. Arai, H. Tou, M. Matsuda, K. Takeda, H. Sugawara, and M.-T. Suzuki, npj Quantum Mater. **8**, 56 (2023).
- 19) K. Momma and F. Izumi, Commission on Crystallogr. Comput., IUCr Newslett., **7**, 106 (2006).
- 20) M. Matsuda, D. Zhang, Y. Kuwata, Q. Zhang, T. Sakurai, H. Ohta, H. Sugawara, K. Takeda, J. Hayashi, and H. Kotegawa, Phys. Rev. B **104**, 174413 (2021).
- 21) M. Yatsushiro, H. Kusunose, and S. Hayami, Phys. Rev. B **104**, 054412 (2021).
- 22) J. Zhao, Z. Shu, and R. S. Dissanayaka Mudiyansele, W. Xie, and T. Kong, Magnetism **2**, 179 (2022).
- 23) T. Miyasato, N. Abe, T. Fujii, A. Asamitsu, S. Onoda, Y. Onose, N. Nagaosa, and Y. Tokura, Phys. Rev. Lett. **99**, 086602 (2007).
- 24) M. Lee, Y. Onose, Y. Tokura, and N. P. Ong, Phys. Rev. B **75**, 172403 (2007).
- 25) N. Manyala, Y. Sidis, J. F. Ditsa, G. Aeppli, D. P. Young, and Z. Fisk, Nat. Mater. **3**, 255 (2004).

1) N. Nagaosa, J. Sinova, S. Onoda, A. H. MacDonald, and N. P. Ong, Reviews of Modern Physics **82**, 1539 (2010).

- 26) H. Toyosaki, T. Fukumura, Y. Yamada, K. Nakajima, T. Chikyow, T. Hasegawa, H. Koinuma, and M. Kawasaki, *Nat. Mater.* **3**, 221 (2004).
- 27) J. S. Higgins, S. R. Shinde, S. B. Ogale, T. Venkatesan, and R. L. Greene, *Phys. Rev. B* **69**, 073201 (2004).
- 28) Liu, E. K. et al. *Nat. Phys.* **14**, 1125 (2018).
- 29) T. Chen, T. Tomita, S. Minami, M. Fu, T. Koretsune, M. Kitatani, I. Muhammad, D. Nishio-Hamane, R. Ishii, F. Ishii, R. Arita, and S. Nakatsuji, *Nat. Commun.* **12**, 572 (2021).
- 30) X. Li, L. Xu, L. Ding, J. Wang, M. Shen, X. Lu, Z. Zhu, and K. Behnia, *Phys. Rev. Lett.* **119**, 056601 (2017).
- 31) M. Ikhlas, T. Tomita, T. Koretsune, M.-T. Suzuki, D. Nishio-Hamane, R. Arita, Y. Otani, and S. Nakatsuji, *Nat. Phys.* **13**, 1085 (2017).
- 32) L. Ding, J. Koo, L. Xu, X. Li, X. Lu, L. Zhao, Q. Wang, Q. Yin, H. Lei, B. Yan, Z. Zhu, and K. Behnia, *Phys. Rev. X* **9**, 041061 (2019).
- 33) W. H. Meiklejohn and C. P. Bean, *Phys. Rev.* **105**, 904 (1957).
- 34) J. Nogués and I. K. Schuller, *J. Mag. Mag. Mat.* **192**, 203 (1999).
- 35) E. Lachman, R. A. Murphy, N. Maksimovic, R. Kealhofer, S. Haley, R. D. McDonald, J. R. Long, and J. G. Analytis, *Nat. Commun.* **11**, 560 (2020).
- 36) A. Noah, F. Toric, T. D. Feld, G. Zissman, A. Gutfreund, D. Tsruya, T. R. Devidas, H. Alpern, A. Vakahi, H. Steinberg, M. E. Huber, J. G. Analytis, S. Gazit, E. Lachman, and Y. Anahory, *Phys. Rev. B* **105**, 144423 (2022).